Spectral enhancements associated with Pi1B events observed at high latitude

Matthew A. Young,[1,2] Marc Lessard,[1] Mark Engebretson,[3] Jesse R. Woodroffe,[4,5] and Kjellmar Oksavik[6]

Received 17 May 2012; revised 8 August 2012; accepted 9 August 2012; published 19 September 2012.

[1] Spectral enhancements observed in conjunction with Pi1B by a ground-based search-coil magnetometer located at Longyearbyen in Svalbard, Norway, are examined as evidence of resonant structures in the ionosphere excited by broadband ultra low frequency geomagnetic micropulsations. We examine the morphology of spectral enhancements in dynamic Fourier spectra using a series of 102 Pi1B events recorded from February through October, 2008, followed by a quantitative analysis of a 49-event subset that allows us to derive an estimate of the range of quality factors that can be expected for Pi1B-associated spectral enhancements. Finally, we use European Incoherent Scatter (EISCAT) radar electron density data recorded during two Pi1B events from the original data set-one during a sunlit ionosphere and one during a dark ionosphere-in conjunction with Mass-Spectrometer Incoherent Scatter (MSIS) and International Model Ionosphere (IRI) model data as input to a model of eigenmodes of the ionospheric Alfvén resonator. We compare the results of this model to the observed spectra and show that the observations can be partially explained as (instantaneous) resonant frequencies of the ionospheric Alfvén resonator.

Citation: Young, M. A., M. Lessard, M. Engebretson, J. R. Woodroffe, and K. Oksavik (2012), Spectral enhancements associated with Pi1B events observed at high latitude, *J. Geophys. Res.*, *117*, A09314, doi:10.1029/2012JA017940.

1. Introduction

[2] A companion paper, *Young et al.* [2012] (henceforth referred to as Paper 1), examined the propagation characteristics of Pi1B events in the high-latitude ionosphere above Svalbard, Norway. Figure 8 in that paper (repeated here as Figure 1) suggests that persistent band-limited enhancements are observed concurrently with Pi1B events in dynamic Fourier spectra, and that there is an annual variation in observations of persistent enhancements correlated with the amount of sunlight incident upon the Svalbard ionosphere. These observations echo early observations made by *Heacock* [1967]. That author noted that the midfrequency of the so-called '4-sec' (i.e. 0.25 Hz) enhancements observed at College, AK (CGM 64.6°N) was nearer to 0.3 Hz during summer nights, moved up in frequency (reaching 1 Hz) in the fall, and was usually not at all visible in winter. Furthermore, College, AK spectral enhancements were especially clear during weak Pi1B bursts. Finally, he observed that amplitudes of spectral enhancements showed a ratio of East-West versus vertical amplitudes over three times greater than that of other impulsive, storm-related activity. Therefore, such enhancements were likely signatures of transverse hydromagnetic waves.

[3] *Arnoldy et al.* [1998] also recorded spectral enhancements associated with Pi1B in Antarctic data and observed that those enhancements were not seen in space by GOES 9. However, whereas the results presented by *Heacock* [1967], indicate a "consistent lack" of 0.3 Hz enhancements during periods of continuous, nonimpulsive, irregular wave power (PiC), *Arnoldy et al.* [1998] suggested that simultaneous PiC and Pi1B wave power results in such enhancements. It is not clear whether *Arnoldy et al.* [1998] observe a process at southern polar latitudes distinct from that observed by *Heacock* [1967] at northern auroral latitudes or *Arnoldy et al.* [1998] include the few-second enhancements in their definition of PiC. In the present study, we shall use the term spectral enhancement to refer to the '4-sec enhancement' phenomenon identified by *Heacock* [1967] as distinct from continuous, nonimpulsive PiC events well-correlated with negative bays in *H*.

[4] Observations of spectral resonant structures (SRS) in the range 0.1–5 Hz and their morphology have been made at mid-latitudes by *Yahnin et al.* [2003] and at high-latitudes by

[1]Space Science Center, University of New Hampshire, Durham, New Hampshire, USA.
[2]Now at Department of Astronomy, Boston University, Boston, Massachusetts, USA.
[3]Department of Physics, Augsburg College, Minneapolis, Minnesota, USA.
[4]Department of Physics and Astronomy, University of Minnesota, Twin Cities, Minneapolis, Minnesota, USA.
[5]Department of Physical Sciences, Embry-Riddle Aeronautical University, Daytona Beach, Florida, USA.
[6]Department of Physics and Technology, University of Bergen, Bergen, Norway.

Corresponding author: M. A. Young, Department of Astronomy, Boston University, Boston, MA 02215, USA. (may@bu.edu)

0148-0227/12/2012JA017940

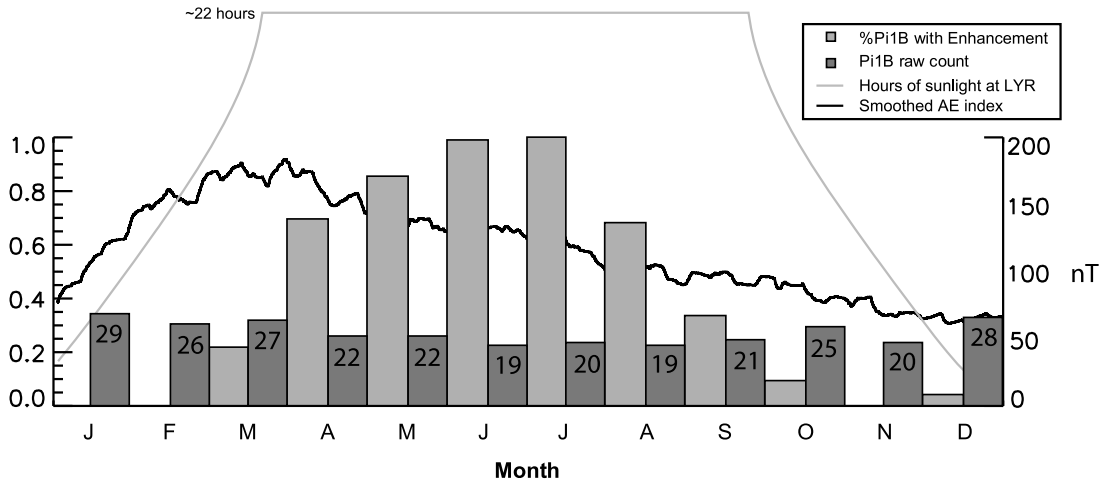

Figure 1. The relationship between the occurrence probability of narrowband enhancement and the number of Pi1B events, hours of sunlight, and the AE index for 2008. The AE index has been smoothed using a boxcar window ~70 days wide.

Belyeav et al. [1999], *Hebden et al.* [2005], *Semenova et al.* [2008], *Semenova and Yahnin* [2008], and *Parent et al.* [2010]. Such observations included banded spectral structures with multiple harmonics that the authors attribute to the ionospheric Alfvén resonator (IAR) as first predicted by *Polyakov* [1976] and first observed by *Belyaev et al.* [1987]. However, *Yahnin et al.* [2003] noted that SRS are "rarely observed during pronounced broadband ULF activity," whereas the spectral enhancements we observe are always associated with a Pi1B event. This suggests that the mechanism responsible for spectral enhancements reported here differs, at least in part, from that responsible for SRS.

[5] The theory of *Lysak* [1988, 1991, 1993, 1997] provides a well-established model of the ionospheric Alfvén resonator. It predicts eigenfrequencies in the 0.1–1.0 Hz range that scale with the ratio of the Alfvén speed to the scale height of the ionosphere above the E region. The resonator is bounded below by the conducting E region, and above by a steep increase in the Alfvén speed ($V_A = B/\sqrt{\mu_o \rho}$) produced by density that goes as $\rho \sim e^{-r}$ and a magnetic field that goes as $B \sim r^{-3}$. It was shown specifically in *Lysak* [1991] that resonant frequencies also correspond to minima of the ionospheric reflection coefficient.

[6] A second resonator model, proposed by *Pilipenko et al.* [2002], is assumed to exist approximately co-spatially with the ionospheric Alfvén resonator during periods of enhanced auroral precipitation. This resonator beneath the auroral acceleration region (RAAR) is bounded below by the conducting E region (as with the IAR) and above by a field-aligned potential drop. Eigenmodes of the RAAR also scale with the ratio of the Alfvén speed to the scale height of the resonator, though the scale height of the RAAR may not necessarily match the scale height of the IAR. In this model, *Pilipenko et al.* [2002] found that values of field-aligned resistance in the $10^7 - 10^9\ \Omega \cdot m^2$ range are typical, and that for values in this range, a field-aligned potential drop of $\Delta\Phi \cong 10 - 10^3$ V is necessary to support a field-aligned current $j_{||} \cong 10^{-6}$ A/m^2. We note in comparison to this that model results from *Chaston et al.* [2002] indicate that pile-up of the wave electric field over the altitudes ~4000 km–8000 km due to electron acceleration creates a standing wave with parallel potential drop of order a few keV for a "short time".

2. Instrumentation

2.1. Location

[7] Induction-coil magnetometer data presented in this paper are drawn from the same data set as that presented in Paper 1. A map showing the Svalbard magnetometer array in geographic coordinates, with the location of the system at Longyearbyen (LYR) indicated by a dashed rectangle, is shown in Figure 2. The Longyearbyen induction-coil magnetometer is located at geographic latitude and longitude 78.20 N and 15.83 E, (2008 corrected geomagnetic latitude and longitude 75.29 N and 111.71 E). It was thus located at an L-shell of 15.70, with magnetic local time (MLT) midnight at 20:50 UT, during this study. The present paper uses data from this station only.

2.2. Equipment

[8] The ULF induction-coil magnetometer deployed at Longyearbyen, Svalbard, consists of 160,000 turns of copper wire wound around an annealed mu-metal core. University of New Hampshire ULF induction-coil magnetometers measure vector *dB*/*dt* along geomagnetic North-South and East-West directions with a −3 dB corner at 2.5 Hz and a resolution of 10 pT/$\sqrt{\text{Hz}}$ over the range of frequency response, which we shall take to mean ~0.001−2.5 Hz in this work. The sampling rate is 10 Hz. Supporting electronics include a coil-mounted preamplifier (gain of 121), as well as main electronics located in the research station ~200 meters away, which are responsible for bandpass filtering and amplification (gain of 244). The overall system sensitivity is 4.43 V · nT^{-1} · Hz^{-1}. Data acquisition electronics and software perform analog-to-digital conversion and data storage, and a GPS antenna/receiver synchronizes data acquisition with 100 μs accuracy. A

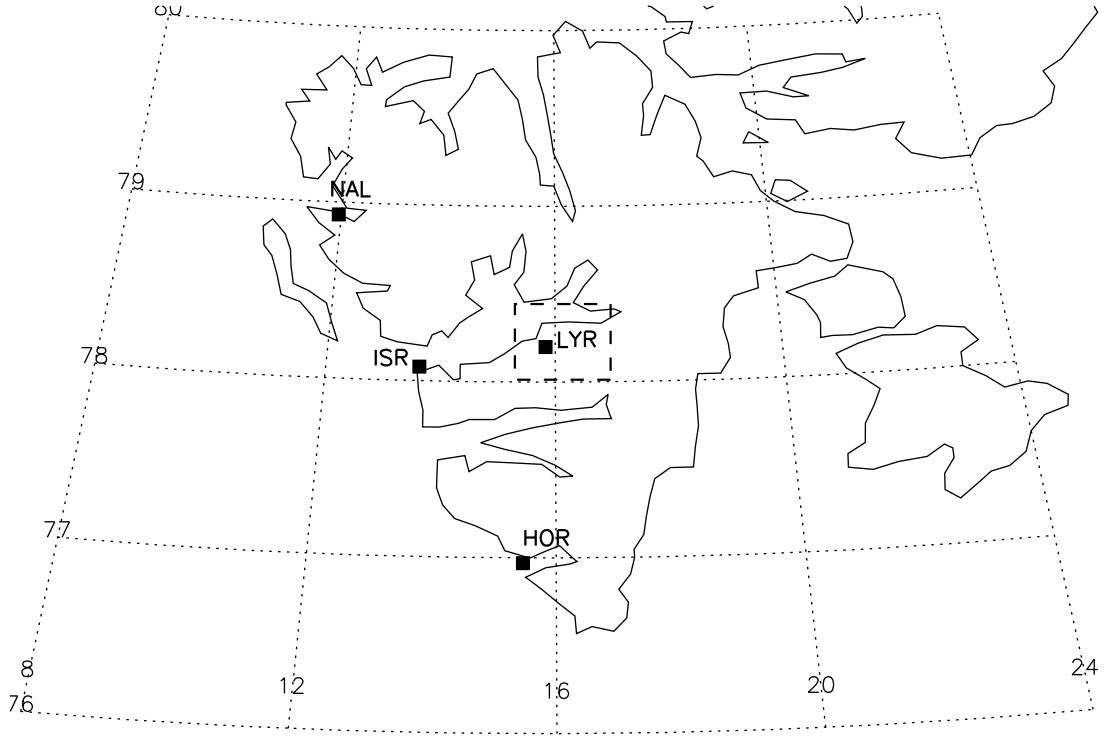

Figure 2. Location of induction coil magnetometers in the Norwegian territory of Svalbard. The station at Longyearbyen (LYR), which was used exclusively in this paper, is indicated by a dashed-line box. Latitude and longitude are given in geographic coordinates.

complete description of this induction-coil magnetometer system can be found in *Kim* [2010].

3. Enhancements Observed at Longyearbyen

[9] We first examine observations of spectral enhancements associated with Pi1B observed at Longyearbyen, as shown in dynamic Fourier spectra. The Fourier spectra were computed via fast Fourier transform (FFT) using a Hanning window 2048 points wide and a time step of 6 s. A subset of these events will then be used to experimentally estimate expected values of the resonator quality factor.

3.1. Event Identification

[10] For the study presented in Paper 1, we identified Pi1B events that occurred within ±3 hours of magnetic local time midnight (MLTMN) by visual inspection of dynamic Fourier spectra produced by the UNH Longyearbyen induction-coil magnetometer in 2008. The advantage of constraining the time period to MLTMN ±3 was that it allowed us to align this study with previous work by *Posch et al.* [2007], and to make contact with previous studies assessing the relationship between Pi1B and substorm processes [e.g., *Arnoldy et al.*, 1998], while excluding similar but unrelated events, such as those studied by *Anderson et al.* [1995] and *Dyrud et al.* [1997].

[11] The original full data set considered in Paper 1 consisted of 102 Pi1B events observed by all three Svalbard magnetometers in 2008 (a subset of the 278 events recorded by at least one Svalbard magnetometer, as shown in Figure 1). The present study attempts to characterize spectral enhancements observed concurrently with Pi1B events in this data set, but the absence of incoherent scatter radar data near Hornsund and Ny Ålesund stations required us to limit our analysis to those Pi1B events observed by the Longyearbyen induction-coil magnetometer.

3.2. Characteristics of the Data Set

[12] Section 4.4 of Paper 1 included a figure (there, Figure 8) that illustrated the relative occurrence of spectral enhancements with respect to the total number of Pi1B events observed by at least one Svalbard magnetometer (278 events), as a function of month in 2008. That graphic, reproduced here as Figure 1, also includes the number of hours during which the ionosphere above Svalbard was sunlit, as well as the AE index, smoothed with a boxcar window ~70 days wide. There is a clear trend toward more observations of Pi1B-related spectral enhancements in summer months. The fact that the distribution is slightly asymmetric about June and July may be related to asymmetry in the AE index, since the AE index is a proxy for substorm activity and Pi1B events typically accompany substorms.

[13] In Figure 3, we have compressed dynamic half-hour Fourier spectra encompassing each of the 102 Pi1B events into a chronological sequence and identified each event by its Day of Year (DOY, from 001 through 366 in 2008). Beginning in the upper left-hand corner and progressing along each row, we see qualitative features of Pi1B with and without enhancements over the period 10 February 2008 (DOY = 041) to 15 October 2008 (DOY = 289) on an aggregate level. The key feature to notice is the morphology of spectral enhancements over the ~8-month period. Enhancements are occasionally evident around 0.6–0.8 Hz in mid-February to early March DOY = 041–065, but they tend to be short-lived in comparison to the duration of Pi1B wave power (see

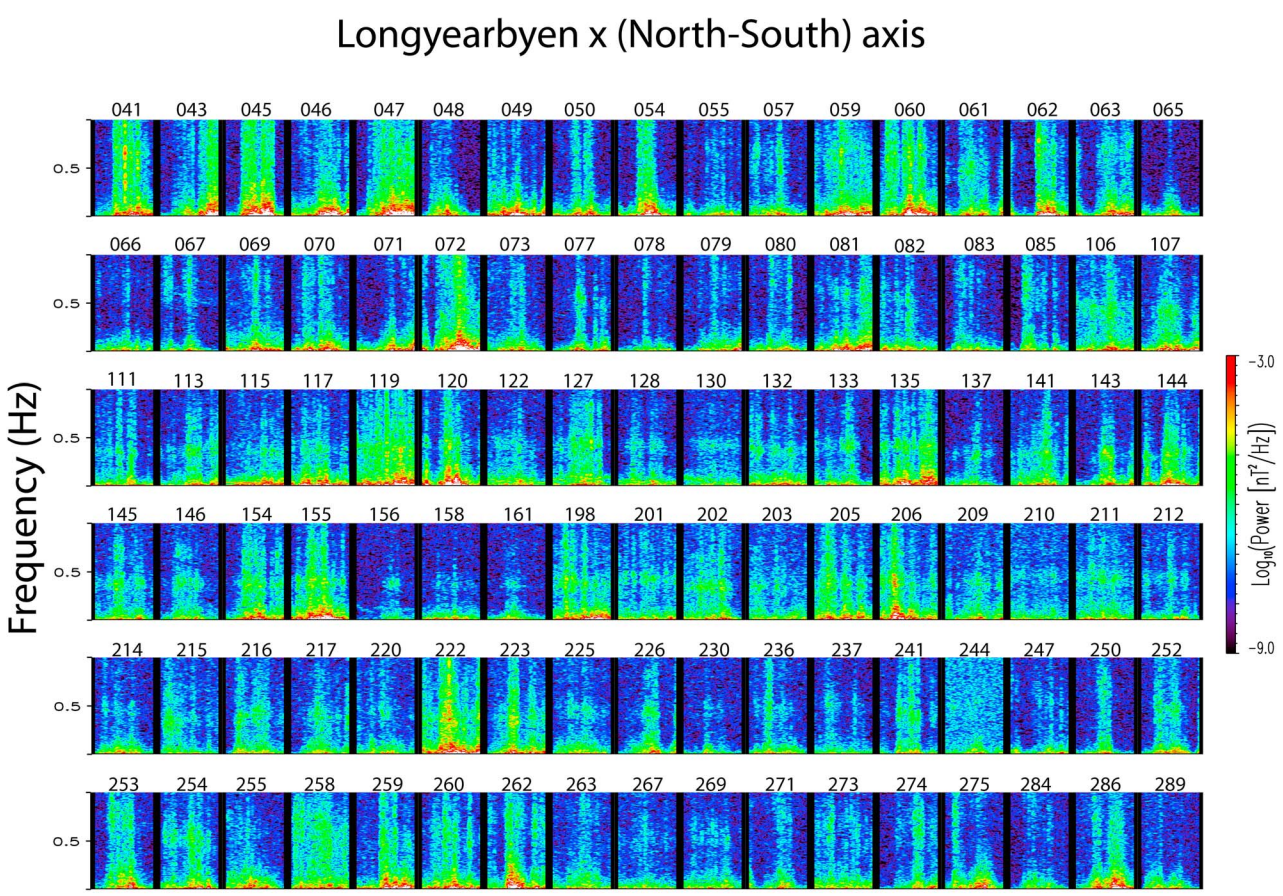

Figure 3. Chronological sequence of 102 events considered in the current study. Time progresses row-wise from 10 February 2008 (Day of Year 041) to 15 October 2008 (Day of Year 289). This graphic illustrates qualitatively the morphology of spectral resonance structures associated with Pi1B events.

explanation of "short-lived" in the following paragraph). Beginning in roughly mid-April (DOY = 111), enhancements are more persistent (again, see the following paragraph) and tend to have a more consistent central frequency of ~0.4 Hz. By late August (DOY = 237), the central frequency has drifted up to ~0.5 Hz and enhancements become more difficult to identify visually. During some Pi1B events near the end of the data set (DOY > 267), some spectral power enhancements may exist, but their frequency range is typically wide enough (greater than 0.2 Hz) or their spectral power weak enough (an order of magnitude or less above background) that distinguishing them from broadband Pi1B power is difficult.

[14] As examples of the difference between "short-lived" and "persistent" enhancements, we have reproduced the half-hour dynamic spectra from days 059 (29 February), 062 (2 March), 132 (11 May), and 202 (20 July) in Figure 4. We note the spectral power enhancement at $f \approx 0.7$ Hz and $f \approx 0.8$ Hz on 29 February and 2 March, respectively, in contrast to the $f \approx 0.4$ Hz on both 11 May and 20 July (color values are the same as given in Figure 3). The enhancements on 29 February and 2 March, which occurred in a dark ionosphere, are more than an order of magnitude more powerful than concurrent broadband power, and exhibit durations of a few minutes. On the other hand, the enhancements on 11 May and 20 July, which occurred in a sunlit ionosphere, are approximately an order of magnitude more powerful than concurrent broadband power, but persist for nearly the entire half-hour period shown. These characteristics result in an apparent increase in spectral enhancements during the sunlit months when data is viewed over long time ranges as in Figure 3. It is perhaps more accurate to say that spectral enhancements at $f \approx 0.3$–0.4 Hz, (e.g. those originally observed by *Heacock* [1967]) are more persistent during sunlit events.

3.3. Estimate of Quality Factor

[15] Every resonator has an associated quality factor Q given by [*Jackson*, 1999]

$$Q = \omega_0 \left(\frac{\text{Stored energy}}{\text{Power loss}} \right) \tag{1}$$

Equation (1) can be recast in terms of a given central frequency and the width of a resonance about that central frequency:

$$Q = \frac{f_0}{\delta f} \tag{2}$$

where δf is the full width at half-maximum of the power curve near f_0. That is, it is the difference in frequency between the two frequency points at which wave power is half its

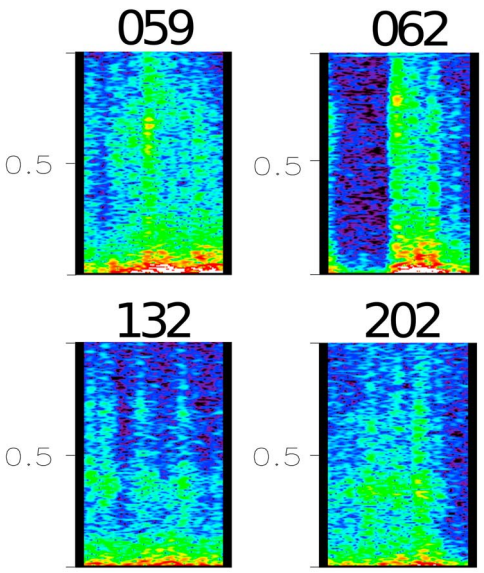

Figure 4. Four examples from Figure 3 that illustrate the difference between short-lived enhancements observed during periods of prolonged darkness (top row, DOY = 059, 062) versus persistent enhancements observed during periods of prolonged sunlit (bottom row, DOY = 132, 202).

maximum (resonant) value. In order to experimentally estimate the quality factor of the IAR during the summer (when spectral enhancements are most obvious, as discussed in section 3.2), we selected a characteristic event on which to perform the following analysis: First, we identified a time of interest by visually inspecting the spectrogram for spectral enhancements, and extracted the wave power spectrum $P(f)$ at that time. Second, we identified the approximate central frequency and frequency range of the spectral enhancement and smoothed $P(f)$ over that range, using a 14 mHz-wide boxcar window. Third, we made an initial estimate for the central frequency, and fit the smoothed data to a Gaussian-plus-quadratic function of the form

$$P_F(f) = a_0 \exp\left[-\frac{1}{2}\left(\frac{f-a_1}{a_2}\right)^2\right] + a_3 + a_4 f + a_5 f^2 \qquad (3)$$

whereby we were able to identify the quantities $f_0 = a_1$ and $\delta f = a_2 \cdot 2\sqrt{2\ln(2)}$. Finally, we computed the quality factor according to equation (2). (Note that use of equation (3) implicitly assumes that the spectral enhancement was sufficiently Gaussian-like after smoothing, and that the background power in the frequency range of interest could be described by a quadratic in the frequency).

[16] Figure 5 is a graphical representation of the estimation process, performed for a Pi1B-associated spectral enhancement observed at Longyearbyen on 4 June 2008. Figure 5a shows x-axis (North-South) Dynamic Fourier spectra for frequencies up to 1.0 Hz between the hours 19:00 and 19:30 UT, with an enhancement with central frequency just below 0.4 Hz between approximately 19:12 and 19:17. Figure 5b shows spectral power at 19:13 UT (black) and spectral power smoothed with a 14 mHz-wide boxcar window (red). Figure 5c shows a close up of Figure 5b between the frequencies 0.3–0.5 Hz. In Figure 5c, raw induction-coil magnetometer data have been plotted in black, while smoothed data and the Gaussian-plus-quadratic fit have been plotted in red and blue, respectively. We see from Figure 5c that, though the fit to the raw spectrum does not correctly identify the frequency of maximum power (an error attributable to the fact that the spectral enhancement does not possess the symmetry about a central frequency of a pure Gaussian), it does capture the behavior of the data well enough to provide a useful estimate of Q. For the event shown in Figure 5, we find that f_0 = 0.383 Hz and δf = 0.0614, and thus Q = 6.23.

[17] Using the above method, we attempted to estimate the quality factor of all 102 events in our data set. After visual inspection of the 102 resultant fits, we found that only 49 Gaussian fits appeared to capture the approximate shape of the spectral peak in the raw data. That is, only 49 apparent spectral peaks were reasonably well-approximated by equation (3). This set of 49 quality factors, with their corresponding central frequencies, is shown in Figure 6. Figure 6 suggests that there may be a trend toward lower quality factors and lower central frequencies in the summer (i.e. inversely proportional to hours of sunlight), but we must be cautious with drawing such a conclusion based on the 49-event subset. Most importantly, these estimates are derived from snapshots of magnetic activity and do not give any information about the evolution of resonator parameters over time. We have already noted, in considering the events shown in Figure 4, that spectral enhancements at $f \approx 0.3$–0.4 Hz are more persistent during periods of prolonged sunlight. In the same section (section 3.2), we also noted that increases in spectra power relative to broadband power may exist in events after DOY ≈ 267, but that their wide frequency range (i.e. $\delta f > 0.2$ Hz) relative to the frequency range plotted (i.e. f = 0.0–1.0 Hz) makes them ambiguous as "enhancements". If a researcher were to determine that such relatively broad enhancements should be included in deriving a yearly trend in Q, he or she would likely find that Figure 6 does not agree with his or her analysis. Further study should characterize not only the quality factor and central frequencies of resonances in magnetometer data, but also the temporal morphology of these quantities, ideally in varying sunlit conditions and varying conditions of solar activity.

4. Resonator Spectrum Model

[18] In order to examine the possible connection between broadband bursty emissions and spectral enhancements, EISCAT incoherent scatter radar data of electron density during two Pi1B events were used as input to a model of the ionospheric Alfvén resonator developed by one of the authors (J. R. W.). The numerical model draws from previous work by *Lysak* [1988] [see also *Lysak*, 1993, 1997] and was implemented to determine characteristic frequencies of the IAR above Longyearbyen during each event.

4.1. Description of the Model

[19] Between 100 and 500 km, the EISCAT data provide electron density (with cubic splines used to obtain values at intermediate points). The IRI-2007 model is used to provide ion masses from 100–1000 km and electron densities

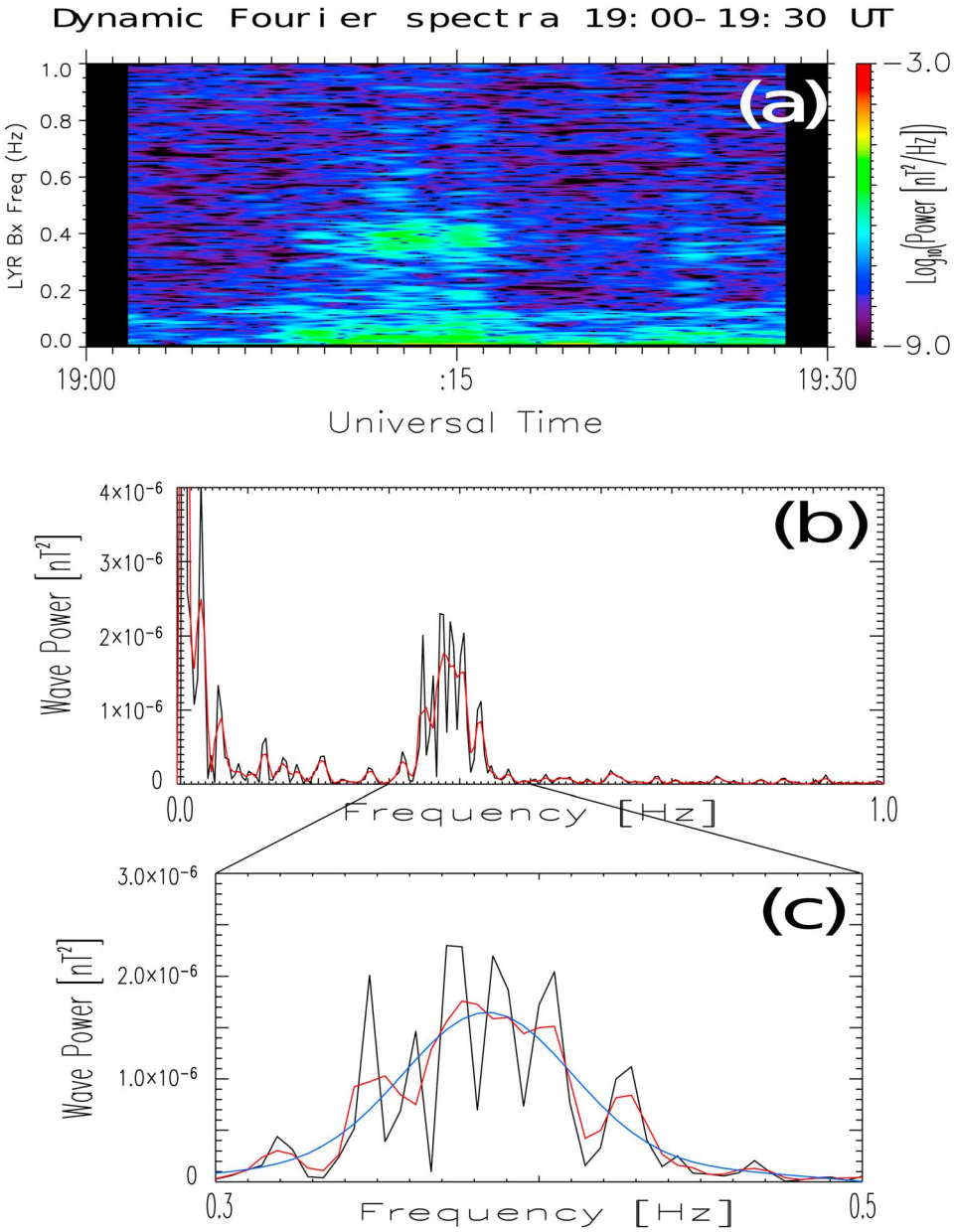

Figure 5. Estimating the quality factor for a spectral enhancement on 4 June 2008: (a) dynamic Fourier spectra from 19:00–19:30 UT, showing the enhancement between 19:12 and 19:17 UT, (b) wave power spectrum at 19:13 UT (black) and data smoothed with a 14 mHz-wide boxcar window (red), and (c) a close-up of the spectral enhancement between 0.3 and 0.5 Hz. In Figure 5c, raw power is plotted in black, smoothed power in red, and the Gaussian-plus-quadratic fit in blue.

between 500 and 1000 km. Above 1000 km, a two-species exponential heavy ion and power-law hydrogen is used, with the scale height and densities derived from the properties of the IRI profile below 1000 km.

[20] In order to calculate the ionospheric conductivities, the IRI-2007 model is used to calculate electron temperature as a function of altitude, and the NRL-MSIS00 model is used to find the neutral particle densities. Combined with our model of the field-aligned mass density distribution, we calculate the Pedersen conductivities for each component and then vertically integrate the conductivity profile to obtain the Pedersen conductance. Finally, we normalize the Pedersen conductance by the E-region Alfvén conductance, $\Sigma_A = 1/\mu_0 V_A$, i.e. $\bar{\Sigma}_P = \Sigma_P/\Sigma_A$.

[21] *Lysak* [1993] presented a method for determining the resonant frequencies of the IAR based on the use of Elsässer variables, e.g. $Z^{\pm} = E_x \mp V_A B_y$. (It can be shown that these correspond to purely upward or downward propagating Alfvén waves, respectively.) Starting at the ionosphere, the impedance boundary condition $\bar{\Sigma}_P E_x = V_A B_y$ is used to

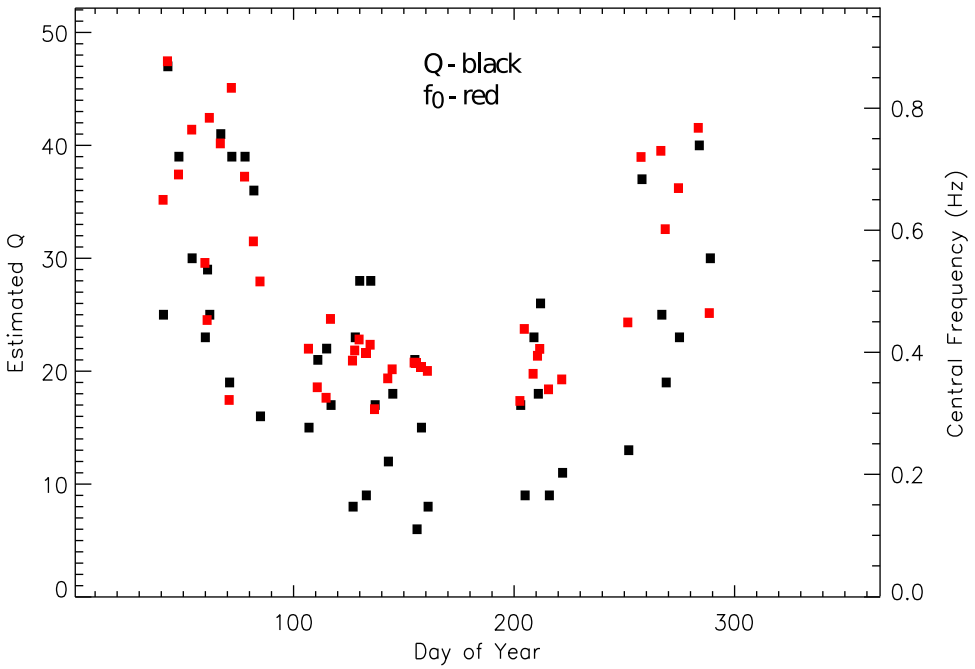

Figure 6. Estimates of 49 quality factors (Q, black), with corresponding central frequencies (f_0, red), plotted as a function of day-of-year (DOY). Values were determined based on individual power spectra and thus do not convey information on the duration of enhancements exhibiting each estimated value of Q. See section 3.3 for discussion.

provide starting values for the time harmonic Alfvén wave equations,

$$\frac{\partial E_x}{\partial z} = i\omega B_y$$

$$\frac{\partial B_y}{\partial z} = i\frac{\omega}{V_A^2}E_x.$$

[22] These equations are integrated from the ionosphere to a distance of a few R_E where the Elsässer variables are evaluated. The reflection coefficient is the ratio of the upward propagating wave to the downward propagating wave, $R = Z^+/Z^-$. The relative amount of wave power that has escaped the IAR (i.e. not been trapped) is quantified by the magnitude of the complex reflection coefficient. The resonant frequencies are identified as those for which the reflection coefficient has a local minimum.

4.2. Comparison Between Model and Observation

[23] We chose two Pi1B events from the original 102 events, one from 3 June 2008 and one from 12 February 2008, to use as a basis for comparison between observations and model results. These events were selected because they represent an event in a sunlit ionosphere and an event in a dark ionosphere, respectively, for which good-quality radar and magnetometer data were available. Dynamic Fourier spectra recorded at Longyearbyen during the time period 18–24 UT are shown in Figures 7a, 7b, 7d, and 7e, where Figures 7a and 7d show x-axis (North-South) dynamic spectral power and Figures 7b and 7e show y-axis (East-West) dynamic spectral power. Figures 7c and 7f show height-integrated Pedersen conductivity (Σ_P, solid line) and Hall conductivity (Σ_H, dashed line) for 3 June and 12 February, respectively. These height-integrated conductivities were computed from the model.

[24] In Figures 7a and 7b, we observe a sequence of Pi1B events on 3 June in both magnetometer components, with the first strong event occurring at 19:30 UT, a second grouping occurring in the range 20:00–20:30 UT, and a third event occurring at 21:15UT. We will focus here on the first powerful event at 19:30. In Figures 7d and 7e, we observe a sequence of Pi1B events on 12 February in x-axis and y-axis components, respectively, that begin at 20:00 UT with a relatively low-power burst, and are followed by a more powerful burst just after 20:15 UT. There is a third burst of broadband power that occurs just before 21:00 UT, but we will again focus on the first powerful event.

[25] Figures 8a–8d present model results for a specific time during each of the two sample dates. The times chosen were 19:30 on 3 June 2008 (Figures 8a and 8c) and 20:18 UT on 12 February 2008 (Figures 8b and 8d); these times will be referred to as the model times in what follows. Figures 8a and 8b show the model ionospheric density at 19:30 UT on 3 June 2008 (Figure 8a) and at 20:18 UT on 12 February 2008 (Figure 8b) used to calculate the height-integrated conductivities presented in Figure 7. Figures 8c and 8d show the ionospheric reflection coefficient as a function of frequency for normalized height-integrated Pedersen conductivity $\Sigma_P/\Sigma_A = 15$ at 19:30 UT on 3 June 2008 (Figure 8c) and for $\Sigma_P/\Sigma_A = 20$ at 20:18 UT on 12 February 2008 (Figure 8d). Superimposed on Figures 8c and 8d as dotted lines are the predicted IAR resonant frequencies, which correspond to minima of the reflection coefficient [*Lysak*, 1993].

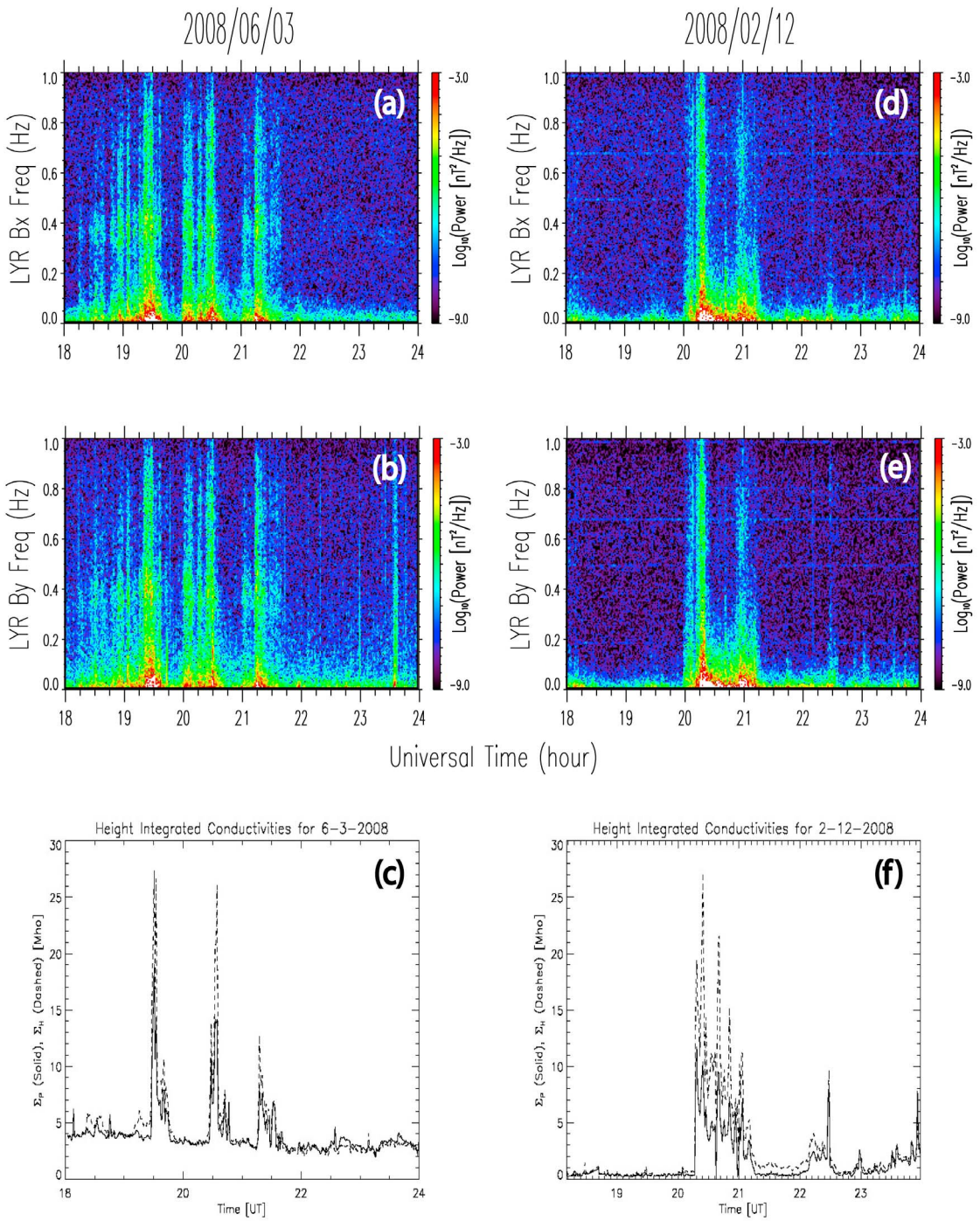

Figure 7. Dynamic Fourier spectra from the Longyearbyen search-coil magnetometer, and height integrated conductivities derived from EISCAT data on two separate dates: (a) x-axis (North-South) spectra on 3 June 2008, (b) y-axis (East-West) spectra on 3 June 2008, (c) height integrated Pedersen (solid) and Hall (dashed) conductivities on 3 June 2008, (d) x-axis (North-South) spectra on 12 February 2008, (e) y-axis (East-West) spectra on 12 February 2008, (f) height integrated Pedersen (solid) and Hall (dashed) conductivities on 12 February 2008.

[26] We now compare these model results to wave power spectra observed during the model times, shown in Figure 9 (the data have been smoothed using the same smoothing routine discussed in section 3.3 in order to highlight spectral peaks). On 3 June 2008 (Figure 9a), there is a distinct spectral peak centered on $f \approx 0.39$ Hz in both x and y components. The reflection-coefficient model (see Figure 8d) predicts a resonant frequency at 0.394 Hz, which agrees very well with observation. The reflection-coefficient model also predicts a resonance at 0.759 Hz that is not visible in magnetometer

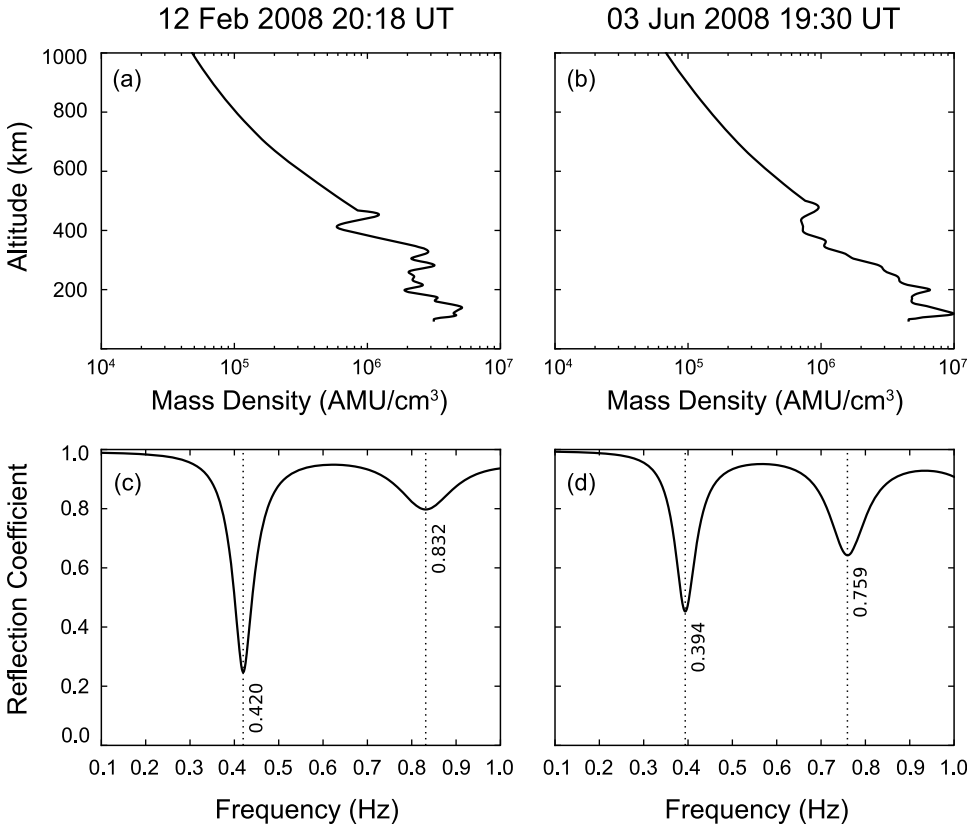

Figure 8. Modeled ionospheric density and reflection coefficient: (a) ionospheric density at 19:30 UT on 3 June 2008, (b) ionospheric density at 20:18 UT on 12 February 2008, (c) reflection coefficient as a function of frequency for $\Sigma_P/\Sigma_A = 15$ at 19:30 UT on 3 June 2008, and (d) reflection coefficient as a function of frequency for $\Sigma_P/\Sigma_A = 20$ at 20:18 UT on 12 February 2008. Predicted IAR resonant frequencies are indicated by dotted lines in Figures 8c and 8d.

data. We note that there appear to be other relatively smaller peaks in spectral power in Figure 9a, but varying the parameters of the FFT caused these apparent peaks to shift, and we thus do not consider them evidence of IAR resonances.

[27] On 12 February 2008 (Figure 9b) there is a clear, narrow spectral peak in y-axis power centered at $f \approx 0.25$ Hz, whereas the reflection-coefficient model predicts a fundamental resonance at 0.420 Hz. While the y-axis spectral peak persists when FFT parameters are varied, we must note that there is not a similar spectral peak in x-axis data (contrast this with Figure 9a, which shows spectral peaks near a predicted resonance in both axes). Thus, this apparent peak wave power may not be the result of IAR resonance. Above ~0.4 Hz, the spectral structure is more complex than that shown in (Figure 9a), with various spectral peaks in both axes, occurring with power less than 1.5×10^{-5} nT^2. However, varying FFT parameters caused these peaks to change and we thus do not consider them evidence of IAR resonances. Therefore, we find that the model predictions and observed data to not match for this snapshot of ULF magnetic activity.

5. Discussion

[28] There is a significant difference in the maximum height to which the perturbed ionospheric structure reaches on 12 February versus 3 June (cf. Figures 8a and 8b up to ≈400 km in altitude), so if the inhomogeneity in Pedersen and Hall conductivities as functions of height ($\sigma_P(z)$ and $\sigma_H(z)$, as opposed to their height-integrated counterparts) contribute to the complexity of spectra observed on the ground, those quantities would have a greater effect during the 12 February event. Additionally, careful examination of Figure 7 suggests that broadband wave power had subsided by 19:30 UT on 3 June to a greater degree than at 20:18 UT on 12 February. Thus the complexity observed in Figure 9b, if not due to IAR resonances, could be due to the persistence of Pi1B wave power that is not present during the spectrum shown in Figure 9a. Furthermore, Alfvénic electron precipitation could lead to momentary build up of field-aligned potential drops as considered by *Chaston et al.* [2002], leading in turn to momentary resonances predicted by the Pilipenko resonator model [*Pilipenko et al.*, 2002] that are in the 0.1–1.0 Hz range but not necessarily identical to resonances predicted by in the Lysak resonator model [*Lysak*, 1988, 1991, 1993, 1997].

[29] We have already remarked (*cf.* section 3.2) that spectral enhancements observed between roughly mid-April through the end of August have more consistent characteristics than those observed during other times of the year. They tend to have a central frequency of ~0.4 Hz, tend to show similar power fall-off on either side of the peak, and

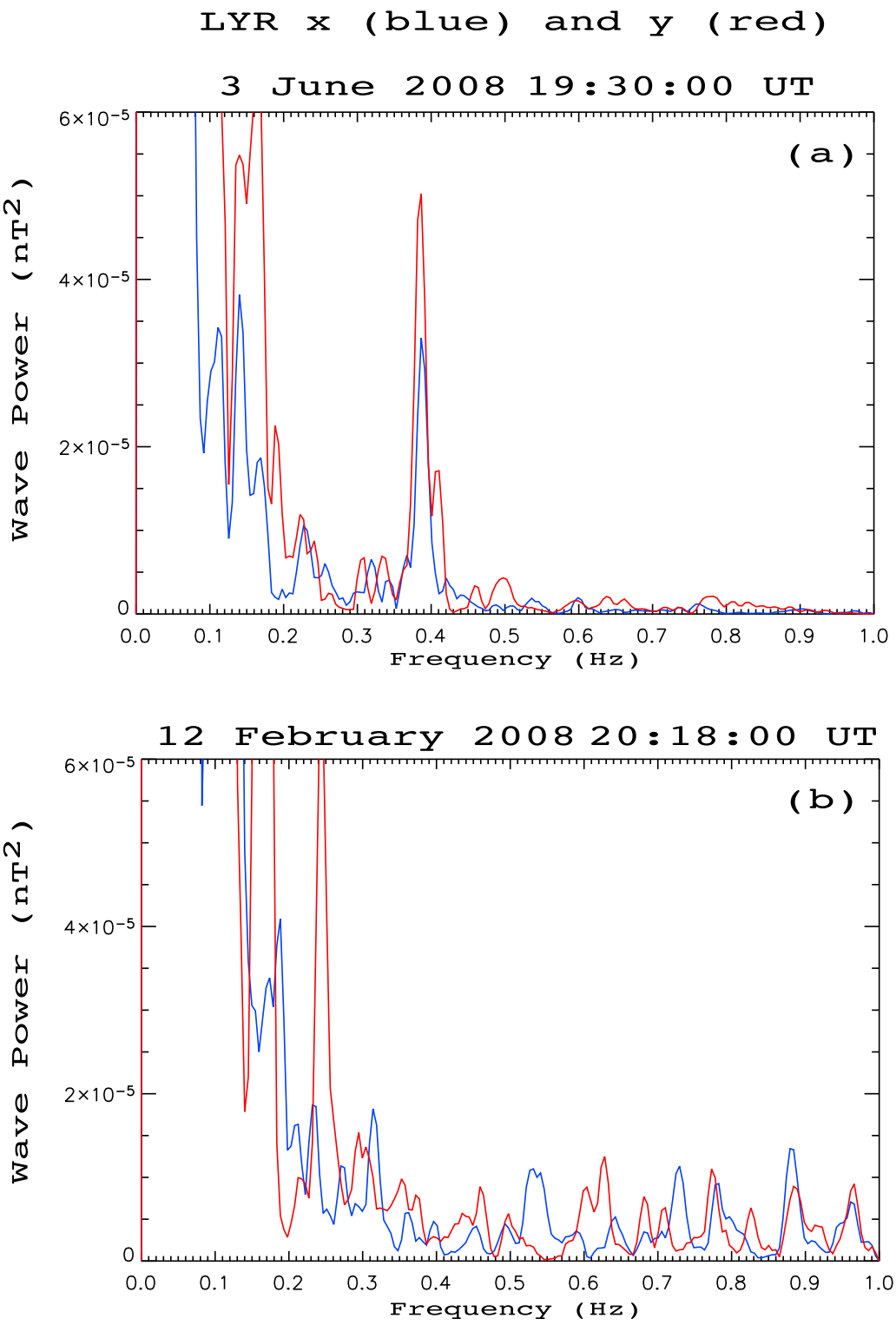

Figure 9. Smoothed Induction-coil magnetometer spectra from (a) 19:30 UT on 3 June 2008 and (b) 20:18 UT on 12 February 2008. In both panels, x-axis (North-South) data have been plotted in blue, while y-axis (East-West) data have been plotted in red. The data were smoothed using a 14 mHz-wide boxcar window.

are a few orders of magnitude higher than spectral power at nearby frequencies. Therefore, the event of 3 June 2008 shown in Figure 9 is representative of most spectral enhancements during this time. On the other hand, the higher degree of variation in spectral enhancements observed outside the mid-April to the end of August period makes identification of representative characteristics difficult. However, inspection of wave power spectra during short intervals reveals that spectral

enhancements do occur in association with Pi1B outside of the summer period, and can exhibit instantaneous quality factors Q as high as ∼40. Further study is needed to determine conclusively if there is any seasonal trend in Q, and to explain why enhancements concurrent with Pi1B in periods of increased sunlight are more persistent despite appearing to exhibit lower resonator quality factors than some short-lived enhancements observed concurrent with Pi1B during periods of darkness. Such further study will require a large amount of good-quality radar and induction-coil magnetometer data recorded at similar times and nearby locations.

6. Summary

[30] In Paper 1, we noted that spectral enhancements were associated with Pi1B events observed at Longyearbyen between the hours of 18–24 UT. A graphic included therein suggested that these events occur more often during periods of prolonged sunlight, in qualitative agreement with *Heacock* [1967] (and with *Arnoldy et al.* [1998] if we assume that those authors use the term "PiC" to refer to the same type of event). After closer study, we can summarize our findings in the following three remarks.

[31] 1. Spectral enhancements (also known as "4-second enhancements") were observed to occur at high latitude in conjunction with Pi1B and to show greater spectral power over longer time ranges during periods of prolonged sunlight (e.g. summer). Thus, they are more easily observable in dynamic Fourier spectra during those periods.

[32] 2. Estimation of the quality factor Q of sample spectral enhancements concurrent with Pi1B events at Longyearbyen suggests that typical values fall between 6 and 40, with values on the high end of that range occurring for short-lived enhancements (∼1 minute) in periods of lessened sunlight (e.g. winter).

[33] 3. A reflection-coefficient model of the ionospheric Alfvén resonator (IAR) eigenfrequencies using ionospheric electron density data from European Incoherent Scatter (EISCAT) radar in Longyearbyen, Norway, was compared to high-latitude ultra low frequency (ULF) induction-coil magnetometer also recorded at Longyearbyen. Comparison of model results to observed data showed that the reflection-coefficient model correctly predicted a spectral-power peak around 0.4 Hz at 19:30 UT on 3 June 2008, but that other predicted resonances were not apparent in magnetometer data.

[34] **Acknowledgments.** Operation of the induction-coil magnetometer at Longyearbyen was supported by NSF grants ARC 0806338 to the University of New Hampshire and ARC 0806196 to Augsburg College. Research at the University of Bergen is supported by the Research Council of Norway. EISCAT is an international association supported by research organizations in Norway (NFR), Sweden (VR), Finland (SA), Japan (NIPR and STEL), China (CRIRP), and the United Kingdom (STFC). Germany (DFG, until 2011) and France (CNRS, until 2005) are earlier EISCAT associates. The authors thank the reviewers for useful comments and critiques.

[35] Robert Lysak thanks the reviewers for their assistance in evaluating this paper.

References

Anderson, H. M., M. J. Engebretson, R. L. Arnoldy, L. J. Cahill Jr., and P. T. Newell (1995), Statistical study of hydromagnetic chorus events at very high latitudes, *J. Geophys. Res.*, *100*, 3681–3692.

Arnoldy, R. L., J. L. Posch, M. J. Engebretson, H. Fukunishi, and H. J. Singer (1998), Pi1 magnetic pulsations in space and at high latitudes on the ground, *J. Geophys. Res.*, *103*, 23,581–23,591.

Belyaev, P. P., S. V. Polyakov, V. O. Rapoport, and V. Y. Trakhtengerts (1987), Detection of resonance structure in the atmospheric electromagnetic noise background spectrum in the range of short-period geomagnetic pulsations, *Sov. Phys. Dokl., Engl. Transl.*, *32*, 983.

Belyeav, P. P., T. Bösinger, S. V. Isaev, and J. Kangas (1999), First evidence at high latitudes for the ionospheric Alfvén resonator, *J. Geophys. Res.*, *104*, 4305–4317.

Chaston, C. C., J. W. Bonnell, C. W. Carlson, M. Berthomier, L. M. Peticolas, I. Roth, J. P. McFadden, R. E. Ergun, and R. J. Strangeway (2002), Electron acceleration in the ionospheric Alfven resonator, *J. Geophys. Res.*, *107*(A11), 1413, doi:10.1029/2002JA009272.

Dyrud, L. P., M. J. Engebretson, J. L. Posch, W. J. Hughes, H. Fukunishi, R. L. Arnoldy, P. T. Newell, and R. B. Horne (1997), Ground observations and possible source regions of two types of Pc 1-2 micropulsations at very high latitudes, *J. Geophys. Res.*, *102*, 27,011–27,027.

Heacock, R. R. (1967), Two subtypes of type Pi micropulsations, *J. Geophys. Res.*, *72*, 3905–3917.

Hebden, S. R., T. R. Robinson, D. M. Wright, T. Yeoman, T. Raita, and T. Bösinger (2005), A qualitative analysis of the diurnal evolution of ionospheric Alfvén resonator magnetic resonance features and calculation of changing IAR parameters, *Ann. Geophys.*, *23*, 1711–1721.

Jackson, J. D. (1999), *Classical Electrodynamics*, 3rd ed., John Wiley, New York.

Kim, H. (2010), Development of ground-based search-coil magnetometer systems in the polar regions and studies of ULF Pc 1–2 wave propagation in the ionospheric waveguide, PhD thesis, Univ. of N. H., Durham.

Lysak, R. L. (1988), Theory of auroral zone Pi1B pulsation spectra, *J. Geophys. Res.*, *93*, 5942–5946.

Lysak, R. L. (1991), Feedback instability of the ionospheric resonant cavity, *J. Geophys. Res.*, *96*, 1553–1568.

Lysak, R. L. (1993), Generalized model of the ionospheric Alfvén resonator, in *Auroral Plasma Dynamics*, edited by R. L. Lysak, pp. 121–128, AGU, Washington, D. C.

Lysak, R. L. (1997), Propagation of Alfvén waves through the ionosphere, *Phys. Chem. Earth, Part B*, *22*, 757–766.

Parent, A., I. R. Mann, and I. J. Rae (2010), Effects of substorm dynamics on magnetic signatures of the ionospheric Alfvén resonator, *J. Geophys. Res.*, *115*, A02312, doi:10.1029/2009JA014673.

Pilipenko, V. A., E. N. Fedorov, and M. J. Engebretson (2002), Alfvén resonator in the topside ionosphere beneath the auroral acceleration region, *J. Geophys. Res.*, *107*(A9), 1257, doi:10.1029/2002JA009282.

Polyakov, S. V. (1976), On properties of an ionospheric Alfvén resonator, in *Symposium KAPG on Solar-Terrestrial Physics*, vol. III, pp. 72–73, Nauka, Moscow.

Posch, J. L., et al. (2007), Statistical observations of spatial characteristics of Pi1B pulsations, *J. Atmos. Terr. Phys.*, *69*, 1775–1796, doi:10.1016/j.jastp.2007.07.015.

Semenova, N. V., and A. G. Yahnin (2008), Diurnal behaviour of the ionospheric Alfvén resonator signatures as observed at high latitude observatory Barentsburg (L = 15), *Ann. Geophys.*, *26*, 2245–2251.

Semenova, N. V., A. G. Yahnin, A. N. Vasil'ev, and O. Amm (2008), Specific features of resonance structures in spectra of ULF electromagnetic noise at high latitudes (Barentsburg Observatory), *Geomagn. Aeron.*, *48*, 36–44.

Yahnin, A. G., N. V. Semenova, A. A. Ostapenko, J. Kangas, J. Manninen, and T. Turunen (2003), Morphology of the spectral resonance structure of the electromagnetic background noise in the range of 0.1–4 Hz at L = 5.2, *Ann. Geophys.*, *21*, 779–786.

Young, M. A., M. Lessard, and M. Engebretson (2012), Pi1B propagation in the high-latitude ionosphere, *J. Geophys. Res.*, *117*, A03322, doi:10.1029/2011JA017127.